How many radio relics await discovery?

S. E. Nuza,[1]⋆ M. Hoeft,[2] R. J. van Weeren,[3] S. Gottlöber[1] and G. Yepes[4]

[1]*Leibniz-Institut für Astrophysik Potsdam (AIP), An der Sternwarte 16, 14482 Potsdam, Germany*
[2]*Thüringer Landessternwarte, Sternwarte 5, 07778 Tautenburg, Germany*
[3]*Leiden Observatory, Leiden University, PO Box 9513, NL-2300 RA Leiden, the Netherlands*
[4]*Grupo de Astrofísica, Universidad Autónoma de Madrid, Cantoblanco, 28039 Madrid, Spain*

ABSTRACT

Upcoming radio telescopes will allow us to study the radio sky at low frequencies with unprecedented sensitivity and resolution. New surveys are expected to discover a large number of new radio sources, in particular those with a steep radio spectrum. Here we investigate the abundance of radio relics, i.e. steep-spectrum diffuse radio emission coming from the periphery of galaxy clusters, which is believed to trace shock waves induced by cluster mergers. With the advent of comprehensive relic samples, a framework is needed to analyse the relic abundance statistically. To this end, we introduce the probability of finding a relic located in a galaxy cluster with given mass and redshift, which allows us to relate the halo mass function of the Universe to radio-relic number counts. To date, about 45 relics have been reported in the literature and we compile the resulting counts, $N(>S_{1.4})$. In principle, the parameters of the distribution could be determined using a sufficiently large relic sample. However, since the number of known relics is still small, for that purpose we use the MareNostrum Universe simulation to determine the relic radio-power scaling with cluster mass and redshift. Our model is able to reproduce the recently found tentative evidence for an increase in the fraction of clusters hosting relics, both with X-ray luminosity and redshift, using an X-ray flux-limited cluster sample. Moreover, we find that a considerable fraction of faint relics ($S_{1.4} \lesssim 10\,\mathrm{mJy}$) reside in clusters with an X-ray flux below $\lesssim 3 \times 10^{-12}\,\mathrm{erg\,s^{-1}\,cm^{-2}}$. Finally, we estimate the number of radio relics that await discovery by future low-frequency surveys proposed for the Low Frequency Array (LOFAR) and the Westerbork Synthesis Radio Telescope (WSRT). We estimate that the Westerbork Observations of the Deep APERTIF Northern-Sky (WODAN) survey proposed for WSRT may discover 900 relics and that the LOFAR–Tier 1–120 MHz survey may discover about 2500 relics. However, the actual number of newly discovered relics will depend crucially on the existence of sufficiently complete galaxy cluster catalogues.

Key words: shock waves – radiation mechanisms: non-thermal – methods: numerical – galaxies: clusters: general – large-scale structure of Universe.

1 INTRODUCTION

Some galaxy clusters show large-scale diffuse radio emission on their outskirts, which apparently does not originate from any individual galaxy. These objects are called 'radio relics'. Spectacular examples have been found, for instance in A3667 (Röttgering et al. 1997), A3376 (Bagchi et al. 2006) and CIZA2242 (van Weeren et al. 2010). Diffuse sources are difficult to detect due to the low surface brightness and steepness of the spectra. Moreover, they can only be classified as relics if galactic foreground and fossil radio

galaxy emission can be excluded and the hosting galaxy cluster is identified. We give a list of currently known relics in Section 4.1.

Radio relics show steep spectral slopes, which suggests that the origin of the radiation is synchrotron emission. Hence, radio relics indicate the presence of both relativistic electrons and magnetic fields. There are several approaches to estimate the strength of the magnetic field in the region of relics. Equipartition arguments have been applied and lead to field strengths in the range ∼0.5–3 μG (Govoni & Feretti 2004). For the northwest relic in A3667, the upper limits of the hard X-ray flux in that region provide a lower bound for the magnetic field, namely 1.6 μG (Nakazawa et al. 2009). The rotation measure (RM) distribution of polarized emission from sources in the cluster volume or the background allows us to constrain the

⋆E-mail: snuza@aip.de

magnetic field strength and the spectrum, leading to magnetic field values of ~1–5 µG (Vogt & Enßlin 2003; Bonafede et al. 2010; Kuchar & Enßlin 2011).

Magnetic fields in galaxy clusters are either primordial (Grasso & Rubinstein 2001) or injected into the protocluster region by active galactic nuclei (AGN) and/or galactic winds (Völk & Atoyan 2000). Whatever the origin of the initial seed, some amplification mechanisms are required to account for its strength in clusters. Cosmological magnetohydrodynamics (MHD) simulations predict a magnetic field strength of the order of µG spread over the cluster volume (e.g. Dolag et al. 2005). These studies indicate that the amplification of the magnetic field resulting from pure adiabatic contraction is not sufficient to explain the observed magnetic field strengths. Merger events and accretion of material on to galaxy clusters are supposed to drive significant shear flows and turbulence within the intracluster medium (ICM). These processes can in principle amplify the magnetic field up to at least µG values (see Dolag, Bykov & Diaferio 2008, and references therein).

The morphology and temperature distribution of the X-ray emission of the clusters that host radio relics indicate that relics only occur in systems with an ongoing or recent merger, e.g. A754 (Macario et al. 2011). For A3667, it has been shown that the relic is located where the bow shock of the moving subclump is expected (Vikhlinin, Markevitch & Murray 2001). For some other clusters, the density and the temperature jump of the shock front at the position of the relic have been identified (see e.g. Markevitch 2010, and references therein). This suggests the following scenario for the origin of large-scale radio relics: cluster mergers lead to the formation of shock fronts, which are responsible of electron acceleration causing the relic radio emission.

Two main mechanisms for the acceleration of electrons have been proposed to explain radio relics: (i) adiabatic compression of fossil radio plasma by the shock wave (Enßlin & Gopal-Krishna 2001; Enßlin & Brüggen 2002) or (ii) diffusive shock acceleration (DSA) by the Fermi I process (Drury 1983; Blandford & Eichler 1987; Jones & Ellison 1991; Enßlin et al. 1998; Malkov & O'C Drury 2001). In the first scenario, radio relics should have toroidal and complex filamentary morphologies showing very steep, curved radio spectra due to inverse Compton (IC) and synchrotron losses. In the DSA scenario, the electrons are accelerated by multiple crossings of the shock front (in a first-order Fermi process) tracing shocks in the case of ubiquitous magnetic fields. It is worth noting that other alternative scenarios have also been suggested (e.g. Keshet 2010).

The formation of radio relics in cosmological simulations has been studied e.g. by Hoeft et al. (2008), Battaglia et al. (2009) and Skillman et al. (2010). The latter studied structure-formation shocks present in two cosmological boxes with a comoving volume of $64^3\,h^{-3}\,\mathrm{Mpc}^3$ and $200^3\,h^{-3}\,\mathrm{Mpc}^3$ and use the non-thermal DSA radio model of Hoeft & Brüggen (2007, hereafter HB07) to give an estimation of the radio-relic luminosity function (RRLF) for $z = 0$ and 1 at 1.4 GHz. On the other hand, Cassano et al. (2010), using a Monte Carlo approach, studied the ocurrence of 'radio haloes' in merging galaxy clusters assuming that electrons are re-accelerated through MHD turbulence, posing interesting constraints for the upcoming Low Frequency Array (LOFAR) at 120 MHz. Here we would like to provide the appropiate scalings of the relic radiation with cluster mass and redshift for a given frequency, as well as giving some plausible predictions regarding upcoming radio surveys within the context of the DSA scenario.

Currently, there are several new radio telescopes under construction, in particular for the very low frequency regime. Moreover, several existing telescopes are being fitted with significantly im-

proved receivers or backends. For instance, in the Netherlands and neighbouring countries LOFAR is almost completed. It will allow observers to survey the sky in a frequency range from 30–240 MHz. New receivers and electronics of the Expanded Very Large Array (eVLA) will improve the sensitivity of the Very Large Array (VLA) drastically. The Westerbork Synthesis Radio Telescope (WSRT) will be equipped with focal-plane array receivers, which will be optimized for 1.4-GHz observations. This will increase the field of view significantly and will hence improve the survey speed tremendously, increasing the expected number of relic observations.

In this work we develop a framework to relate the abundance of galaxy clusters in the Universe to radio-relic number counts. To this end we introduce the 'radio-relic probability density', i.e. the probability of finding a radio relic with a given radio power located in a galaxy cluster of given mass and redshift. A large sample of observed relics would allow us to determine the probability density function fully for a given halo mass function in the Universe. However, since only about 45 relics are presently known we therefore use the MareNostrum Universe cosmological simulation as a way of determining how the probability density scales with cluster mass and redshift. In order to normalize this function we compile a list of currently known radio relics.

From the resulting probability distribution, we are also able to reproduce the recently found fractions of clusters with relics in the combined Northern ROSAT All-Sky + ROSAT-ESO flux-limited X-ray (NORAS + REFLEX) cluster sample presented by van Weeren et al. (2011c). Finally, we draw some conclusions on the amount of non-identified relics due to the fact that the hosting cluster is still not known. Moreover, we present some estimates on how many relics may be identified by upcoming radio surveys assuming plausible survey specifications.

This paper is organized as follows. In Section 2 we derive the formalism to estimate the number of radio relics and introduce the 'radio-relic probability function'. We also extend the usually assumed sharp transition for the flux detection limit to a 'discovery probability', which is more appropriate for relic samples. In Section 3 we present the cosmological simulation used in this work and briefly summarize the shock-detection method and the non-thermal radio emission model adopted. In Section 4 we present the most up-to-date observed relic sample, discuss the normalization of our model counts and its comparison with observations and present our predictions for upcoming radio surveys. Finally, in Section 5 we close the paper with a summary.

In what follows we assume a flat ΛCDM cosmology with a matter density parameter $\Omega_M = 0.27$, an amplitude of mass fluctuations $\sigma_8 = 0.8$ and a Hubble constant $H_0 = 100\,h\,\mathrm{km\,s^{-1}\,Mpc^{-1}}$, with $h = 0.7$ (e.g. Komatsu et al. 2011), except when stated otherwise.

2 HOW TO ESTIMATE THE NUMBER OF OBSERVABLE RELICS?

In this section we present the formalism aimed at estimating relic number counts in a given radio survey as well as the radio-relic probability density.

2.1 Cumulative radio-relic number counts

How many relics are seen in the sky above a given radio flux S_ν at the observing frequency ν_{obs}? The flux of a source with luminosity per unit frequency $P_\nu := \mathrm{d}P/\mathrm{d}\nu(\nu)$ located at redshift z is given by

$$S_\nu(P_\nu, z) = P_\nu \frac{1+z}{4\pi d_l^2(z)}, \tag{1}$$

where ν is the rest-frame frequency and $d_l(z)$ is the luminosity distance keeping in mind that the appropriate redshift correction for the frequency between the rest and observer frames needs to be considered.

We introduce the luminosity function of 'radio-relic clusters', i.e. the number of galaxy clusters per unit comoving volume and logarithmic relic radio power as a function of frequency and redshift:

$$n_P(z) := \frac{d^2 N}{dV_c \, d\log P_\nu}(P_\nu, z), \qquad (2)$$

where N is the number of clusters and V_c the comoving volume. The RRLF is obtained by the convolution of a halo mass function, (e.g. Tinker et al. 2008)

$$n_M(z) := \frac{d^2 N}{dV_c \, d\log M}(M, z),$$

with the 'radio-relic probability density' of finding a galaxy cluster of mass M, redshift z and relic radio power P_ν. Therefore, the RRLF becomes

$$n_P(z) = \int_{-\infty}^{\infty} n_M(z) p(P_\nu, M, z) \, d\log M, \qquad (3)$$

where the relic probability density $p(P_\nu, M, z)$ fulfils the following condition

$$\int_{-\infty}^{\infty} p(P_\nu, M, z) \, d\log P_\nu = 1. \qquad (4)$$

Hence, integrating equation (2) allows us to write the total abundance of relics per logarithmic flux bin as follows

$$\frac{dN}{d\log S_\nu}(S_\nu) = \int_0^{\infty} n_P(z) \frac{dV_c}{dz}(z) dz. \qquad (5)$$

Note that we have used $d\log P_\nu = d\log S_\nu$, since P_ν depends linearly on S_ν. In observations, low-luminosity radio relics are hard to identify since the surface brightness may be too low to exhibit typical morphological features or spectral index variations. Moreover, a diffuse radio object is only identified as a relic when the galaxy cluster can be unambiguosly detected. Depending on the mass of the cluster, this may also be challenging. As a consequence, we introduce a 'discovery probability': instead of a sharp flux limit we use a smooth transition, which includes both the sensitivity of the survey and the uncertainties present in the identification. We write this probability as

$$\phi(S_\nu) = \frac{1}{2}\left[1 + \mathrm{erf}\left(\frac{\log S_\nu - \log S_\nu^{\mathrm{eff}}}{w}\right)\right], \qquad (6)$$

where the effective sensitivity, S_ν^{eff}, basically gives the flux limit and w the width of the transition.

Finally, the cumulative radio relic function can be computed by convolving equation (5) with the 'discovery probability' and multiplying by the sky fraction, f_s, covered by the radio survey:

$$N(>\log S_\nu) = f_s \int_{\log S_\nu}^{\infty} \frac{dN}{d\log S_\nu}(S_\nu)\phi(S_\nu) \, d\log S_\nu. \qquad (7)$$

The radio flux–luminosity relation given by equation (1) and the redshift integration of equation (5) are fully determined by the cosmological parameters. Since recent cosmological observations show that the resulting parameters are well-constrained, the procedure described above can be considered as a direct relation between the radio-relic probability density and the observed number counts.

2.2 Radio-relic probability density

If we were to build a perfect radio telescope that could detect even the faintest radio emission, which radio-power distribution function linked to structure formation shocks should we expect? Merger shocks can persist in the cluster periphery basically forever, hence every cluster should show some relic radio emission. On the other hand, very bright and very faint relics are most likely rare events. We therefore expect that there is a typical radio luminosity for a cluster with given mass and redshift, although the related flux is evidently below current detection limits. As a consequence, we assume that the probability density to find a relic is given by a log-normal distribution:

$$p(P_\nu, M, z) \propto \exp\left\{-\frac{(\log P_\nu - \log \bar{P}_\nu)^2}{2\sigma_P^2}\right\}, \qquad (8)$$

where σ_P is the standard deviation of the logarithmic radio power and $\bar{P}_\nu$ is the *mean* radio power, which scales with hosting cluster mass, observed frequency and redshift respectively. We parametrize this function as follows:

$$\log \bar{P}_\nu = \log P_0 + C_M \times \log\left(\frac{M}{10^{14.5}\, h^{-1}\,\mathrm{M}_\odot}\right)$$
$$+ C_z \times \log(1+z) + C_\nu \times \log\left(\frac{\nu_{\mathrm{obs}}}{1.4\,\mathrm{GHz}}\right). \qquad (9)$$

The radio-power normalization is given by the 'reference radio power' P_0 while the scaling with hosting cluster mass, redshift and observing frequency is governed by C_M, C_z and C_ν respectively. Formally, a different functional form could have been chosen for the radio-relic probability density as long as the condition given in equation (4) is fulfilled. However, we will show in Section 3.3 that a log-normal function describes the radio-power distribution of our simulated relic samples reasonably well.

3 SIMULATING RADIO RELICS

In order to simulate radio relics, we need to use a galaxy cluster sample extracted from a cosmological simulation and apply an emission and magnetic model to the present shock waves. In this section we present our cosmological simulation, the method used to detect shocked gas within the simulated volume and our radio-power emission model. Finally, we estimate the parameters of the relic probability density using our cosmological simulation.

3.1 The simulated galaxy cluster sample

Our simulated galaxy cluster sample was selected from the MareNostrum Universe cosmological simulation, which is a non-radiative hydrodynamical run of a representative region of the Universe (Gottlöber & Yepes 2007). The simulation was run with the smoothed particle hydrodynamics (SPH) Gadget-2 code (Springel 2005). The adopted cosmology is in agreement with a flat ΛCDM scenario having a matter density parameter $\Omega_M = 0.3$, a baryon density parameter $\Omega_b = 0.045$, an intial matter power spectrum characterized by a scalar spectral index $n = 1$ and normalized to $\sigma_8 = 0.9$ and a dimensionless Hubble parameter $h = 0.7$. The simulation started at $z = 40$ using a linear density field represented by 2×1024^3 gas and dark matter particles in a comoving box of $500\,h^{-1}$ Mpc on a side. The resulting mass resolution for gas and dark matter particles is $8.3 \times 10^9\,h^{-1}\,\mathrm{M}_\odot$ and $1.5 \times 10^9\,h^{-1}\,\mathrm{M}_\odot$ respectively.

Identification of bound structures is done using the parallel friends-of-friends (FoF) algorithm described in Klypin et al. (1999)

with a linking length of 0.17 in units of the mean interparticle separation. In order to generate our galaxy cluster catalogues as a function of cosmic time, we consider five different redshifts up to $z = 1$, namely $z = 0$, 0.25, 0.5, 0.75 and 1, and take the 500 most massive galaxy clusters present at each cosmic time. In this way, the range of cluster masses we are able to probe goes from $\sim 10^{14} \, h^{-1} \, \mathrm{M}_\odot$ up to $\sim 2.5 \times 10^{15} \, h^{-1} \, \mathrm{M}_\odot$, meaning that the baryonic component of the systems inside the virial radius is typically resolved with thousands of gas particles for the less massive clusters and with several tens of thousands for the most massive ones.

3.2 Shock-finding and radio emission in the simulation

The cosmological SPH code GADGET clearly accounts for shock dissipation as shown by shock-tube simulations (e.g. Springel, Yoshida & White 2001). To this end, artificial viscosity has been introduced into SPH, which evaluates the local velocity field for estimating the dissipation (Monaghan 1992). However this technique is not able to determine the Mach numbers, which are needed for combining SPH simulations with parametric models for radio emission of relics. Two methods have been introduced for locating shock fronts and estimating their strength: Pfrommer et al. (2006) uses the increase of entropy with time while Hoeft et al. (2008) evaluates spatial entropy gradients in single snapshots of the simulation. Here we apply a slightly modified version of the latter approach.

Briefly, our scheme for locating shock fronts can be summarized as follows. For a given gas particle we evaluate its pressure gradient and define the *shock normal* of the particle as $\boldsymbol{n} \equiv -\nabla P / |\nabla P|$. In the case in which the pressure gradient corresponds to a true shock front, several conditions must be fulfilled. In particular, we demand that (i) the velocity field shows a negative divergence, (ii) the density increases from the upstream to the downstream region and (iii) the latter is also valid for the entropy. Utilizing the Rankine–Hugoniot jump conditions for hydrodynamical shocks (see e.g. Landau & Lifshitz 1959), these requirements allow us to determine the Mach number $\mathcal{M}_i$. For a conservative estimate we compute the Mach numbers according to all three conditions and then take the minimum. We wish to avoid the overestimation of the Mach number, since this could lead to spurious strong radio emission. We apply this shock-detection scheme to all gas particles inside a cube of size $10 \, h^{-1} \, \mathrm{Mpc}$ (comoving) centred in the centre of mass of the systems available in our FoF catalogues. We consider here merger shocks, i.e. shocks introduced by cluster mergers, which are found to have typical Mach numbers around ~ 2.5–3 (Araya-Melo et al. 2011). We note also that fast galaxies in a rather cold ICM may generate shock fronts.

In order to predict the radio power of the simulated shock fronts, we need to know the magnetic field strength in the downstream area of the shock fronts. Following our previous work in Hoeft et al. (2008) and that of Skillman et al. (2010), we assume that the magnetic field is given by

$$B = B_0 \times \left(\frac{n_\mathrm{e}}{10^{-4} \, \mathrm{cm}^{-3}} \right)^\eta, \tag{10}$$

where n_e is the local electron density, B_0 is a magnetic field reference value and η is the slope of the density scaling. This dependence is motivated by the assumption that on average the magnetic field in the ICM is frozen-in and that the gas motions distribute the magnetic field even to the outskirts of the cluster where luminous radio relics are generated. In fact, using Faraday rotation measures in the Coma cluster, Bonafede et al. (2010) found evidence that magnetic fields are spread over the entire ICM. In this work we explore two magnetic

models. In the first place we assume $B_0 = 0.1 \, \mu\mathrm{G}$ and $\eta = 2/3$ (e.g. Hoeft et al. 2008), which typically leads to $\sim \mu\mathrm{G}$ values at the ouskirts of galaxy clusters (model 'a'). We also adopt the scaling found by Bonafede et al. (2010), which produces higher magnetic field values ($\gtrsim \mu\mathrm{G}$) at these locations (model 'b'). Their best-fitting model indicates a slightly lower exponent than before, but a stronger field for an electron density of $10^{-4} \, \mathrm{cm}^{-3}$, namely $\eta = 1/2$ and $B_0 = 0.8 \, \mu\mathrm{G}$, respectively. It is worth mentioning that the upper limits for the IC emission in the hard X-ray band for the northwest relic in A3667 indicate higher magnetic field strength ($\geq 1.6 \, \mu\mathrm{G}$: Nakazawa et al. 2009) than obtained here for a typical electron density of $\sim 10^{-4} \, \mathrm{cm}^{-3}$. Hence, this could lead to an overestimation of the hard X-ray flux for a similar relic in the simulation. However, it is not currently known whether the relic in A3667 hosts an exceptionally strong magnetic field or whether relics in general show field strengths of a few $\mu\mathrm{G}$ or more.

As mentioned in the Introduction, the emission scenario (ii) states that thermal (or mildly relativistic) electrons are accelerated at the shock front by DSA. Important evidence for this mechanism comes from the relic in galaxy cluster CIZA 2242 (van Weeren et al. 2010). In this case the observed gradient in the spectral index is consistent with electrons accelerated at the shock front, while synchrotron and IC losses cause the steeper spectral index in the downstream region. The relic in CIZA 2242 also shows that radio emission originates from a rather small volume downstream of the shock front with an extent less than 50 kpc. Based on the DSA model, we have worked out in HB07 how the radio emission is related to the Mach number of the shock, downstream plasma properties and the surface area of the shock front. Assuming that the relativistic electron population is advected with the downstream plasma and cooled down due to synchroton losses and IC scattering with CMB photons, we are able to estimate the total radio emission. In particular, the radio power per unit frequency contributed by a SPH gas particle i can be written as follows:

$$P_{\nu,i} = 6.4 \times 10^{34} \, \mathrm{erg \, s^{-1} \, Hz^{-1}} \, \frac{A_i}{\mathrm{Mpc}^2} \, \frac{n_{\mathrm{e},i}}{10^{-4} \, \mathrm{cm}^{-3}}$$

$$\times \, \frac{\xi_\mathrm{e}}{0.05} \left(\frac{\nu}{1.4 \, \mathrm{GHz}} \right)^{-s_i/2} \left(\frac{T_{\mathrm{d},i}}{7 \, \mathrm{keV}} \right)^{3/2}$$

$$\times \, \frac{(B_{\mathrm{d},i}/\mu\mathrm{G})^{1+s_i/2}}{(B_{\mathrm{CMB}}/\mu\mathrm{G})^2 + (B_{\mathrm{d},i}/\mu\mathrm{G})^2} \, \Psi(\mathcal{M}_i). \tag{11}$$

In this formula, A_i represents the surface area given by the SPH particle, $n_{\mathrm{e},i}$ is the electron density, ξ_e is the electron acceleration efficiency, s_i is the shock compression factor, $T_{\mathrm{d},i}$ is the post-shock temperature, $B_{\mathrm{d},i}$ is the post-shock magnetic field, B_{CMB} is the magnetic measure of the CMB energy density and $\Psi(\mathcal{M}_i)$ is a function that depends on the shock strength.

We note that the efficiency ξ_e for electron acceleration denotes the fraction of the energy dissipated at the shock front that is transferred to suprathermal particles. The lower energy threshold for suprathermal particles is computed from the condition that the power-law distribution of suprathermal electrons must meet the thermal electron distribution at the lower energy threshold; see HB07 for more details. As a result of this approach, the radio emission decreases drastically for Mach numbers lower than 3. For the computations that follow, we simply adopt $\xi_\mathrm{e} = 0.005$. We encourage the reader to see HB07 for more detail.
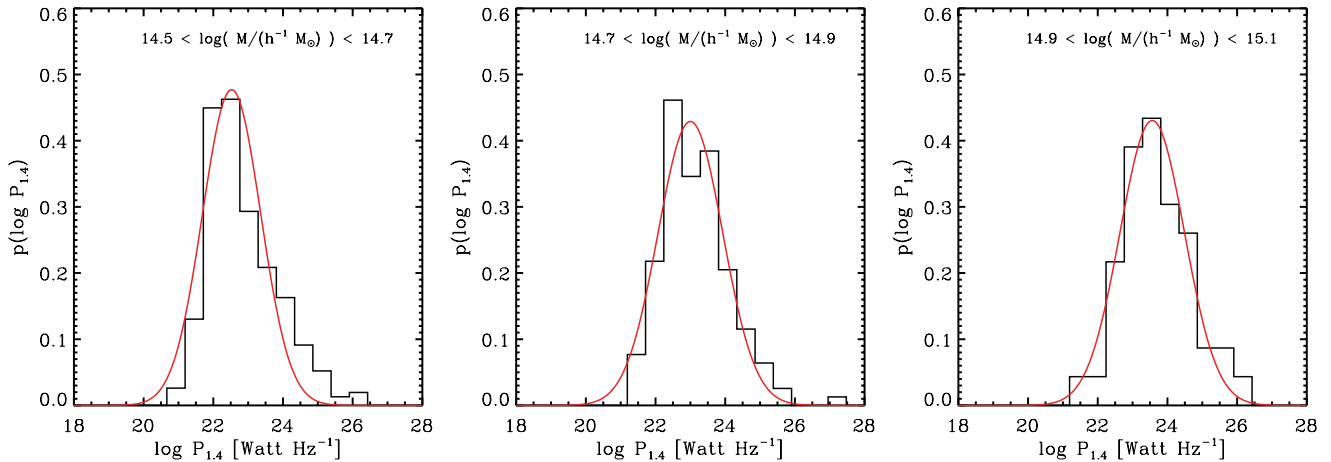
Figure 1. Radio-power probability density for relics inside $3.6\,h^{-1}$ Mpc from the cluster centre at $z = 0$ and observing frequency $\nu_{\rm obs} = 1.4$ GHz (magnetic model 'a'; see text). The histograms show results from hosting haloes belonging to the MareNostrum simulation for three different cluster mass ranges and the solid lines are log-normal fits according to equation (8) normalized using the condition given by equation (4).

3.3 Estimation of the expected radio-power scalings using the MareNostrum Universe

Our aim is to estimate the probability of finding relic radio emission coming from an arbitrary galaxy cluster having mass M, located at redshift z and observed at frequency $\nu_{\rm obs}$. To this aim, we analyse the radio emission produced in the different clusters of our synthetic samples. As mentioned in Section 3.1, we take the 500 most massive clusters at each redshift considered (i.e. $z = 0, 0.25, 0.5,$ 0.75, 1) and identify the shock fronts in each one of them. At all redshifts, we evaluate the radio power emitted from cluster relics as a function of hosting galaxy cluster mass and observing frequency. Note that when computing the radio power we consider all the luminosity caused by structure-formation shocks within a distance of $3.6\,h^{-1}$ Mpc (comoving) from the centre of mass without distinguishing between different relics. However, in each cluster there are typically only one or two prominent relics that contribute most to the final radio emission.

We considered five different frequencies in our analysis, namely $\nu_{\rm obs} = 0.12, 0.15, 0.21, 0.325$ and 1.4 GHz. Fig. 1 shows the radio-power distribution of relics at $z = 0$ and $\nu_{\rm obs} = 1.4$ GHz in the case of magnetic model 'a', where the three panels show results for different hosting cluster mass. The best-fitting log-normal functions are also shown. We explore the parameter space of our relic cluster samples, given by the cluster mass, redshift and observing frequency, and repeat the fitting procedure of Fig. 1 (for simplicity we assume a constant value for σ_P). In this way, we are able to find a set of parameters for the radio-relic probability density capable of reproducing the mean radio-power scalings of our synthetic radio relics (see equation 9). The best-fitting scaling parameters for the two magnetic field models adopted are shown in Table 1. In general, the derived scalings show a good agreement. However, magnetic model 'b' displays lower radio-power scalings with mass and redshift in comparison with model 'a', which is most noticeable for the redshift evolution. The reason for this can be understood in terms of the stronger magnetic field values achieved within the context of magnetic model 'b'. Since according to equation (11) the radio emission saturates for large magnetic field values, the resulting radio-power scaling is not so pronounced in this case.

As can be seen from Fig. 1, log-normal functions reproduce the radio-power distribution of the synthetic relics reasonably well. However, since there are possibly more small shocks, a better reso-

Table 1. Best-fitting parameters for the radio-relic probability density given by equation (8) using our set of MareNostrum clusters for magnetic field scaling models 'a' and 'b' (see text). The reference radio power, P_0, is obtained in our models using the available relic observations for normalization (see Section 4.2). As a comparison, the radio-power scaling parameters obtained by Skillman et al. (2010) in the same redshift range are shown (they assume model 'a' and an acceleration efficiency $\xi_{\rm e} = 0.005$).

	$\log P_0$	C_M	C_z	C_ν	σ_P
This work ('a')	21.35	2.56	3.43	−1.20	0.85
This work ('b')	21.53	2.22	2.49	−1.15	0.85
Skillman et al.	22.20	3.65	3.90	−	−

lution in the simulation may serve to alleviate the observed skewness in the radio-power distribution at low cluster masses. Additionally, this could allow us to extend the cluster mass range studied to estimate the mean radio-power scalings. In the following section we present the currently known observed relic sample to normalize our theoretical expectations further with observations.

4 HOW MANY RELICS DO WE EXPECT?

4.1 Compilation of currently known relics

By definition, relics consist of diffuse radio emission in the periphery of galaxy clusters without any optical counterpart. Hence, relics are commonly searched for by correlating radio surveys with large catalogues of galaxy clusters. The Westerbork Northern Sky Survey (WENSS) has been carried out at 325 MHz covering the north sky for declinations higher than $28.5°$. The noise level of this survey is 3.6 mJy (Rengelink et al. 1997). The National Radio Astronomy Observatory (NRAO) Very Large Array Sky Survey at 1.4 GHz (NVSS) covers the sky north of $-40°$ and has a noise level of 0.45 mJy (Condon et al. 1998). Systematic searches for diffuse radio emission in galaxy clusters have been undertaken, for instance, by inspecting a sample of 205 X-ray bright Abell-type clusters in the NVSS catalogue (Giovannini, Tordi & Feretti 1999), analysing the WENSS data at the position of all Abell clusters (Kempner & Sarazin 2001) and searching for steep-spectrum sources in the VLA

Low-frequency Sky Survey (VLSS: Cohen et al. 2007) catalogue (van Weeren et al. 2009c).

As described above in more detail, current models for the formation of relics are not able to *predict* the actual number of observable relics by themselves, because both the number density of relativistic electrons and the strength of magnetic fields are in general poorly constrained quantities. Therefore, we wish to normalize the radio-relic number counts, $N(>S_\nu)$, using the number of known radio relics. To this end, we have compiled a list of all radio relics reported in the literature, as far as we are aware of, which can be seen in Table 2. We have included all types of radio relics, i.e. Mpc-scale single and double relics in the periphery of clusters as well as smaller relics inside the cluster volume. A few of the small relics might be attributed to the compression of fossil radio plasma (known as the 'radio phoenix' class in the terminology of Kempner et al. 2004). However, we do not include phoenixes when computing the relic number counts.

For each cluster in Table 2 we give the flux of the diffuse emission, which has been classified as 'relic' while the contribution of radio haloes has been excluded. In the cases in which halo and relic radio

Table 2. List of currently known relics extracted from the literature. Columns: (1) cluster name, (2) classification (R: single relic; D: double relic; P: phoenix; C: diffuse radio emission detected (more observations are needed to confirm its nature); F: probably misclassified as relic), (3) radio flux (all relics in the cluster are considered), (4) observed frequency, (5) redshift, (6) radio power (computed assuming a spectral index of -1.2), (7) radio-power deviation (model 'a'; see text), (8) cluster X-ray luminosity, (9) cluster X-ray temperature, (10) checkmark if within NVSS relic sample ($\delta > -40°$), (11) checkmark if within NORAS+REFLEX cluster sample (in brackets if below flux limit $S_R = 3 \times 10^{-12}$ erg s^{-1} cm^{-2}), (12) references (radio/X-ray).

Cluster	Type	$S_{1.4}$ [mJy]	ν_{obs} [GHz]	z	$P_{1.4}$ $\times 10^{24}$ [W Hz^{-1}]	ΔP [σ_P]	L_X $\times 10^{44}$ [erg s^{-1}]	T_X [keV]	NVSS	N+R	References[a]
0217+70	C	-	-	0.0655	-	-	0.25	-	✓		Br11
0809+39	C	62.6	1.4	-	-	-	-	-	✓		BR09
1RXS 06+42	R	357.8	1.38	0.225	52.69	2.36	10.0	-	✓		vWp
24P73	P	12.0	1.38	0.16	0.86	-	-	-	✓		vW11a
A S753	C	460.0	1.4	0.014	0.20	4.32	0.04	-	✓		Su03/B04
A13	P	35.5	1.4	0.0940	0.81	2.07	1.24	6.8	✓	✓	S01/B04
A85	P	40.9	1.4	0.0555	0.30	0.39	5.18	6.4	✓	✓	S01/M98
A115	R	14.7	1.4	0.1971	1.71	0.25	15.70	5.5	✓		Go01
A133	P	137.0	1.4	0.0566	1.05	2.12	1.40	4.3	✓	✓	S01/B04
A521	R	14.1	1.4	0.2475	2.75	1.10	7.44	7.0	✓	✓	Gi08/B04
A523[b]	C	64.0	1.43	0.1034	1.70	2.74	0.89	-	✓	✓	vW11c/B00
A548W	R	121.0	1.4	0.0424	0.51	3.91	0.11	-	✓	(✓)	F06/B04
A610	C	18.6	1.4	0.0956	0.44	-	-	-	✓		GF00
A725	C	6.0	1.4	0.0900	0.12	1.47	0.80	-	✓		KS01/B00
A746	R	24.3	1.38	0.2323	4.05	1.89	3.68	-	✓	✓	vWp
A754	R	6.0	1.37	0.0542	0.04	-0.39	3.79	9.0	✓	✓	Ma11/M11
A781	C	15.0	1.4	0.2952	4.56	1.83	4.15	9.9	✓	(✓)	Go11,V08,V11
A786	F	120.0	1.48	0.1241	5.31	2.87	1.53	-	✓		GF00/B00
A1240	D	16.1	1.4	0.159	1.16	2.39	1.00	4.8	✓		B09/D99
A1300	R	15.0	1.4	0.3075	4.89	0.96	12.12	13.9	✓	✓	R99
A1612	R	62.0	1.4	0.1797	5.80	2.46	2.41	-	✓	✓	vW11c/B04
A1664	D	107.0	1.4	0.1276	4.72	1.46	7.20	-	✓	✓	Go01
A1758	C	12.8	1.4	0.2799	3.32	0.86	10.90	7.0	✓		G09/E98
A2034	C	23.6	1.38	0.1130	0.79	1.15	3.56	7.2	✓	✓	vW11c/E98
A2048	P	18.9	1.43	0.0972	0.47	1.44	1.90	-	✓		vW11a/Sh08
A2061	R	26.7	1.38	0.0784	0.41	0.75	3.95	4.5	✓		vW11/E98
A2163	R	18.7	1.4	0.2030	2.33	0.21	19.62	11.8	✓	✓	F01/B04
A2255	R	43.0	1.4	0.0809	0.70	1.24	3.08	6.1	✓	✓	PD09/E98
A2256	R	462.0	1.4	0.0581	3.96	1.49	3.69	6.9	✓	✓	CE06/E98
A2345	D	59.0	1.4	0.1760	5.35	2.01	3.91	-	✓	✓	Bo09/B04
A2744	R	18.2	1.4	0.3066	5.97	1.09	11.68	9.2	✓	✓	Go01
A3365	R	50.0	1.43	0.0926	1.12	2.55	0.86	-	✓		vW11c/B04
A3376	D	302.0	1.4	0.0468	1.52	2.60	1.01	4.3		✓	Ba06/Ma98
A3667	D	4000.0	1.4	0.055	29.21	3.46	2.18	6.5		✓	R97/Ma98
A4038	P	49.0	1.4	0.0292	0.10	1.23	1.00	3.1	✓		S01/B04
CIZA0649+18	R	31.6	1.43	0.064	0.32	1.08	2.38	-	✓		vW11c/E02
CIZA2242+53	R	241.0	1.38	0.1921	26.05	2.34	6.80	5.8	✓		vW10/K07,Op
COMA	R	229.2	1.4	0.0231	0.28	0.68	3.63	8.3	✓	✓	G91/RB02
MACS 0717+37	R	142.3	1.43	0.5548	200.44	1.98	32.90	10.5	✓		vW09a,Bo09/Ed03
MaxBCG 138.9	C	24.7	1.4	0.32	8.87	-	-	-	✓		vW09c
MaxBCG J217+13	P	19.6	0.61	0.16	0.53	1.68	0.79	2.1	✓		vW09c/O11
PLCK G287.0	D	58.0	1.4	0.39	33.51	1.62	17.20	12.9	✓		Ba11

Table 2 – *continued*

Cluster	Type	$S_{1.4}$	ν_{obs}	z	$P_{1.4}$ $\times 10^{24}$	Δ_P	L_X $\times 10^{44}$	T_X	NVSS	N+R	References[a]
		[mJy]	[GHz]		[W Hz^{-1}]	[σ_P]	[erg s^{-1}]	[keV]			
RXC 1053+54	R	20.0	1.43	0.0704	0.25	2.37	0.44	-	✓	✓	vW11c/P04
RXC 1314-25	R	35.2	1.4	0.2439	6.68	1.31	9.92	-	✓	✓	V07/B04
ZwCl 0008+52	D	67.0	1.38	0.104	1.86	3.25	0.50	-	✓		vW11b
ZwCl 2341+00	R	28.5	1.4	0.27	6.85	3.17	1.10	5.0	✓		vW09b,G10/Ba02

[a]Ba02: Bagchi et al. (2002), Ba06: Bagchi et al. (2006), Ba11: Bagchi et al. (2011), Bo00: Böhringer et al. (2000), B04: Böhringer et al. (2004), Bo09: Bonafede et al. (2009), Br11: Brown, Duesterhoeft & Rudnick (2011), BR09: Brown & Rudnick (2009), CE06: Clarke & Ensslin (2006), D99: David, Forman & Jones (1999), E02: Ebeling, Mullis & Tully (2002), Ed03: Edge et al. (2003), F01: Feretti et al. (2001), F06: Feretti et al. (2006), Gi08: Giacintucci et al. (2008), G91: Giovannini, Feretti & Stanghellini (1991), G09: Giovannini et al. (2009), G10: Giovannini et al. (2010), GF00: Giovannini & Feretti (2000), Go01: Govoni et al. (2001), Go11: Govoni et al. (2011), K07: Kocevski et al. (2007), KS01: Kempner & Sarazin (2001), M98: Markevitch et al. (1998), M03: Markevitch et al. (2003), Ma11: Macario et al. (2011), Op: Ogrean et al. (in prep.), O11: Ogrean et al. (2011), P04: Popesso et al. (2004), PD09: Pizzo & de Bruyn (2009), V07: Venturi et al. (2007), vW09a: van Weeren et al. (2009a), vW09b: van Weeren et al. (2009b), vW09c: van Weeren et al. (2009c), vW10: van Weeren et al. (2010), vW11a: van Weeren et al. (2011a), vW11b: van Weeren et al. (2011b), vW11c: van Weeren et al. (2011c), vWp: van Weeren et al. (in prep.), RB02: Reiprich & Böhringer (2002), R97: Röttgering et al. (1997), R99: Reid et al. (1999), S01: Slee et al. (2001), Sh08: Shen et al. (2008), Su03: Subrahmanyan et al. (2003), V08: Venturi et al. (2008), V11: Venturi et al. (2011).
[b]Giovannini et al. (2011) has classified this source as a radio halo.

emission are on top of each other due to projection effects, we only estimate the flux density of the relic emission. In many clusters the diffuse relic emission is fragmented into multiple pieces (e.g. A2255: Pizzo et al. 2008) or shows some prominent patches and very extended emission as well (e.g. CIZA 2242: van Weeren et al. 2010). Instead of separating individual relics in a single galaxy cluster, we combine the flux, S_ν, of all relics in the cluster, which is consistent with defining the radio luminosity probability for diffuse radio emission in clusters instead of that for relics (in the same way as done in Section 3.2). For our analysis it is not useful to introduce relics as self-contained objects, since their identification depends inevitably on observational parameters such as sensitivity and resolution. Hence, we give in column (3) of Table 2 the entire radio relic flux present in each cluster. To normalize the relic number counts, $N(S_\nu)$, we use the cluster flux at 1.4 GHz because most of the measurements available are done in the 21-cm band. We also estimate the radio power of the relics at 1.4 GHz (see column 6 of Table 2) assuming a spectral slope of -1.2, which is consistent with the parameter C_ν given in Table 1. Interestingly, A3667 displays an outstanding high flux. However, this object is not the most radio-luminous relic, as can be seen in Table 2. The ten most luminous relics have fluxes $S_{1.4} \gtrsim 100$ mJy. It is worth noting that several of these luminous relics have been detected in recent years, namely 1RXS 06, CIZA 2242 and MACS 0717. On the other hand, the faintest relics known to date have a flux of $\sim$6 mJy.

4.2 Normalizing the radio-relic number counts

Basically, we would like to normalize the predicted radio-relic number counts by using the bright end of the observed number-count distribution. As noted above, amongst the ten brightest relics there are however three relics that have been identified only recently. This could indicate that even the bright end of the relics list does not contain all bright relic sources on the sky, which may introduce an offset in the global counts. Hence, in order to estimate number counts we assume a fiducial flux of 100 mJy to centre the discovery probability. This means that at $S_{1.4}^{eff} = 100$ mJy half of the radio relic emission has been detected. Although this choice is arbitrary, we take this value as a compromise between the lowest and brightest relics in the observed distribution. Furthermore, since the lowest flux of known radio relics is of a few mJy, we can set $w = 0.8$, which

ensures that the discovery probability virtually vanishes below these values.

The non-detection of a relic could be due to several reasons. For instance, part of the sky might not be covered by deep radio surveys, galactic foreground radiation or bright sources in the cluster may obscure the diffuse emission, the surface brightness of the diffuse emission may be too low or the related cluster could have not yet been identified. All these possibilities for the non-detection of existing diffuse radio patterns in a galaxy cluster are included in the complementary discovery probability $1 - \phi$.

Since we already have a model for the relic discovery probability, we are now able to normalize the number counts to the present observed sample (which we dub as 'NVSS' since many candidates have been found by means of that survey). In order to do so, we take from Table 2 all confirmed relics above a declination of $-40°$ without including phoenixes. As can be seen in Fig. 2, the observed
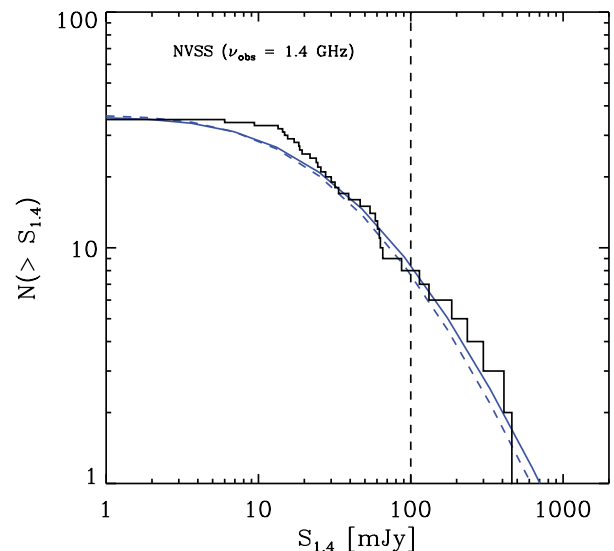

Figure 2. Cumulative number of NVSS radio relics. The histogram shows the observed relic sample while the solid and dashed lines show our magnetic models 'a' and 'b' normalized to number counts at $S_{1.4}^{eff} = 100$ mJy (vertical dashed line). The normalization leads to log $P_0 = 21.35$ and 21.53 respectively (see Section 4.2).

number of radio relics is well reproduced when using a normalization given by $\log P_0 = 21.35$ and 21.53 for magnetic models 'a' and 'b' respectively. However, a degeneration between the normalization parameter and the detection threshold exists: a higher value for the normalization would imply a threshold higher than 100 mJy if one is willing to reproduce observations. This would mean that the majority of relics with this higher flux has not been detected yet. We consider this possibility unlikely. On the other hand, we will show below that within the context of the magnetic models considered here a lower normalization can be ruled out as a result of the analysis of an X-ray flux-limited cluster sample and their associated relics. The obtained low reference radio power ($\log P_0 \sim 21.4$) is enough to describe the observed distributions reasonably (see Section 4.3). Therefore, for the set of parameters derived above for the relic radio-power probability (C_M, C_z, C_ν, σ_P) we are able to constrain the normalization very well.

It is worth noting that to determine radio powers for the simulated clusters we had to *assume* an acceleration efficiency $\xi_e = 0.005$ (with ξ_e as defined in the HB07 model) and we had to *assume* average scalings for the magnetic field, see equation (10). For our MARENOSTRUM clusters, these assumptions lead to a reference radio power of $\log P_0 = 22.23$ and 24.13 in the case of magnetic models 'a' and 'b' respectively. Since, as mentioned above, to reproduce observations we require lower values for the normalization, this implies that the acceleration efficiency must be $\xi_e \lesssim 0.001$. In particular, for model 'b' the observed acceleration efficiency could be about $\xi_e \sim 10^{-5}$, which is more in line with theoretical expectations of DSA in Type Ia supernova remnants (Edmon et al. 2011). Further increase of the magnetic field values, as suggested by Nakazawa et al. (2009), would reduce the required efficiency even more.

Most of the observed radio relics have a redshift lower than 0.3. In the sample there are only five relics with higher redshift, and only one of them is located at $z > 0.5$. We wish to compare these numbers with the predictions according to the radio-relic probability distribution. We simply split the result into the redshift intervals given above, as can be seen in Fig. 3. Apparently, our models predict more relics than observed for $z > 0.3$. This might indicate that relics in distant clusters are more difficult to detect (e.g. due to resolution effects), clusters need to be more X-ray luminous to be found or our scaling parameter C_z derived from the simulations does not agree with the actual redshift evolution. In particular, model 'b' seems to reproduce observations better at all redshifts. However, it is important to realize that the number of both predicted and observed relics with $z > 0.3$ is very small, so we should be cautious of any

interpretation. Much more extensive catalogues of relics are needed to draw a significant conclusion about the redshift evolution.

The most distant cluster that hosts a relic is MACS 0717. Fig. 3 indicates that in our model the highest redshift relics should have fluxes $S_{1.4}$ within the range 10–50 mJy. Instead, the relic in MACS 0717 has a flux of about 140 mJy, indicating that this system is an outstanding radio relic. In fact, it is the most luminous relic known to date with $P_{1.4} \cong 2 \times 10^{26}$ W Hz^{-1}. For instance, using scalings resulting from magnetic model 'a', the mean relic radio power of clusters having the mass and redshift of MACS 0717 is $\bar{P}_{1.4} \cong 4.1 \times 10^{24}$ W Hz^{-1} (see equation 9). Hence, the luminosity of the relic is about $2\sigma_P$ higher than the mean relic luminosity, so it is a rare event but still reasonably likely considering all clusters in the Universe.

In general, we can study the deviation between the estimated radio power from observations and the expected mean radio power at a given redshift and cluster mass. We can quantify this deviation in terms of $\Delta_P := \log\left(P_{1.4}/\bar{P}_{1.4}\right)/\sigma_P$, which measures the difference between the logarithmic radio power estimated from observations and the peak of the radio-relic probability distribution in units of the parameter σ_P. In order to make a simple estimate, we adopt the cluster X-ray luminosities given in column (8) of Table 2 to compute the cluster masses. In what follows we use a L_X–M relation similar to that given by Pratt et al. (2009), which will be presented in Section 4.4. In column (7) of Table 2 we give Δ_P for all relics in our observed sample, adopting the scalings derived with the magnetic model 'a' to estimate the mean radio power. As expected, most of the relics display a mean deviation of $\sim 2\sigma_P$ since we are observing the brightest (or close by) relics in the sky. Some of the relics show an unexpected high deviation from the mean radio power, $\bar{P}_{1.4}$, given by the hosting cluster mass and redshift. This may serve as an indication of the need to investigate these systems further in more detail to confirm their relic nature. However, the large deviations may also come from uncertainties in the cluster mass estimate. We do not pretend here to give a rigorous derivation of the hosting cluster masses but only assess the global tendency of the sample.

4.3 The X-ray–radio power relation

For giant radio haloes in massive galaxy clusters, a close correlation between radio power and X-ray luminosity has been found (e.g. Venturi et al. 2007). Moreover, Enßlin & Röttgering (2002) suggested that the radio power of haloes scales with the X-ray
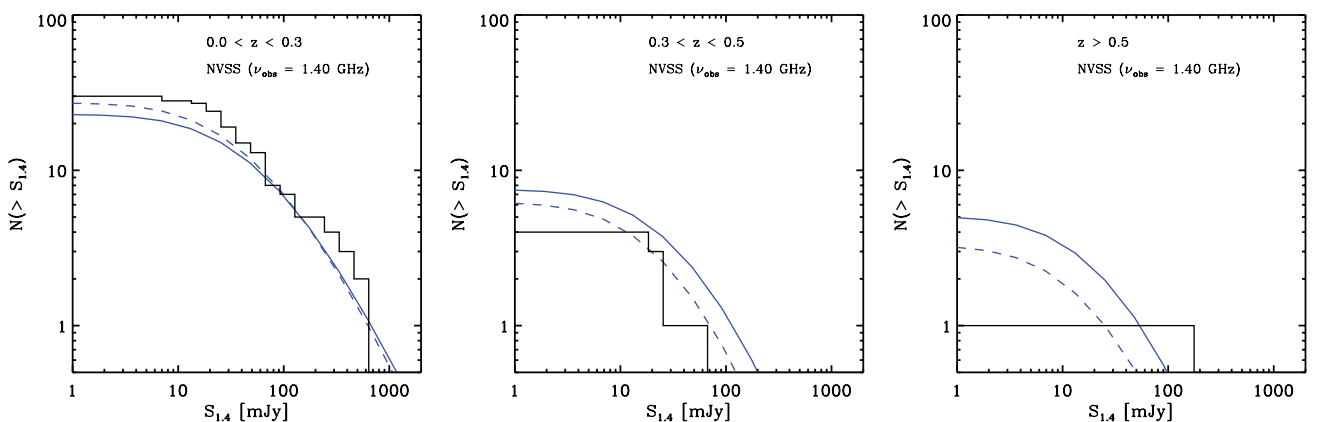

Figure 3. Cumulative number of NVSS radio relics for different reshift bins. The histograms show results for the NVSS radio-relic sample presented in this work, while solid (dashed) lines show the outcome of our magnetic model 'a' ('b').
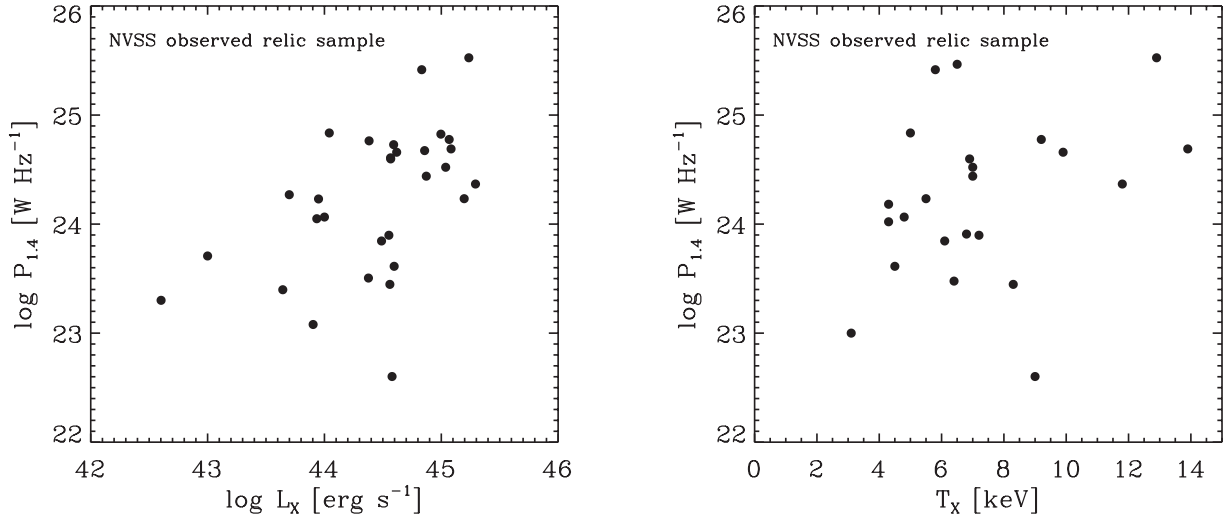
Figure 4. Estimated relic radio power at 1.4 GHz as a function of X-ray cluster luminosity (left panel) and temperature (right panel) for the NVSS relic sample. All X-ray quantities are derived in the *ROSAT* 0.1–2.4 keV band (see Table 2).

luminosity of the clusters according to

$$\frac{P_\nu^{\text{halo}}(L_X)}{10^{24}\,\text{W Hz}^{-1}} = a_\nu \left(\frac{L_X}{10^{45}\,\text{erg s}^{-1}}\right)^{b_\nu}, \tag{12}$$

with parameters $a_\nu = 5.36$ and $b_\nu = 1.69$. In contrast, the radio power of relics show a large scatter for a given X-ray luminosity or temperature, as can be seen in Fig. 4. This fact precisely reflects the starting point of this work, namely the recognition that the radio power of relics varies strongly for a given galaxy cluster mass. Therefore, this motivated us to introduce the radio-power probability distribution. Formally, we can relate the mean radio power, $\bar{P}_{1.4}$, to the X-ray luminosity of clusters at $z = 0$ using the L_X–M relation in equation (9) for the parameters given in Table 1. Comparing this result with equation (12), we obtain for a_ν and b_ν the values 1.3×10^{-3} and 1.5, respectively. Interestingly, we find a similar exponent but a much lower proportionality constant. This seems to indicate that there are much less bright radio relics than haloes. However, we have to keep in mind that when computing the RRLF not only the *mean* radio power but also the radio-power distribution function needs to be taken into account (see equation 3). As a consequence we expect more radio relics than haloes, as can be seen in Fig. 5.

4.4 Radio relics and an X-ray-selected cluster sample

The radio-power probability density introduced above allows us to predict the fraction of clusters in an X-ray-selected sample that hosts a radio relic. As a first step, we introduce the differential distribution with respect to cluster X-ray flux:

$$n_{S_X S_\nu} := \frac{\text{d}^2 N}{\text{d} \log S_X\, \text{d} \log S_\nu}. \tag{13}$$

In a similar way to equation (5), we can write

$$n_{S_X S_\nu} = \int_0^\infty n_M(z)\, p(P_\nu, M, z)\, \frac{\text{d} \log M}{\text{d} \log S_X}\, \frac{\text{d} V_c}{\text{d} z}\, \text{d} z. \tag{14}$$

Note that radio power is a function of radio flux and redshift; similarly, the X-ray luminosity is a function of X-ray flux and redshift. Using the L_X–M relation (see below) to estimate the cluster mass based on its X-ray luminosity, we can write $p(P_\nu, M, z) = p(P_\nu(S_\nu, z), M(S_X, z), z)$. We now introduce an X-ray flux threshold, S_X^{th},
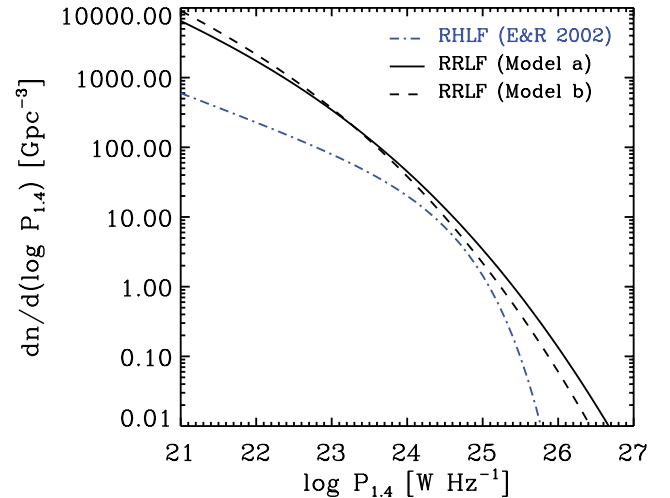

Figure 5. Luminosity function of radio relics for models 'a' and 'b' (solid and dashed lines respectively) and radio haloes (dot–dashed line) at 1.4 GHz and $z = 0$. The radio halo luminosity function is an analytic approximation taken from Enßlin & Röttgering (2002) under the assumption that a constant fraction $f_{\text{rh}} = 1/3$ of the clusters contain radio haloes.

and assume that only clusters with a flux above the threshold are detected. This allows us to determine the cumulative fraction of clusters with $S_X > S_X^{\text{th}}$ that host diffuse relic emission with a given flux S_ν. Integrating the previous equation leads to

$$F_X(>S_X^{\text{th}}, S_\nu) = \frac{1}{N_X(S_\nu)} \int_{S_X^{\text{th}}}^\infty n_{S_X S_\nu}\, \text{d} \log S_X, \tag{15}$$

where the normalization factor, $N_X(S_\nu)$, is determined by the condition $F_X(>0, S_\nu) = 1$. Fig. 6 shows the cumulative fraction of clusters for three different radio fluxes (for the sake of simplicity we assume only the radio-power scaling parameters that result from model 'a' throughout this section; adopting those of model 'b' do not modify our main conclusions). About 80 per cent of the clusters that host diffuse relics with 100 mJy have an X-ray flux larger than $3 \times 10^{-12}\,\text{erg s}^{-1}\,\text{Hz}^{-1}$, which corresponds to the completeness limit of the REFLEX cluster sample (Böhringer et al. 2004). Since candidate radio relics are commonly identified by cross-correlating radio
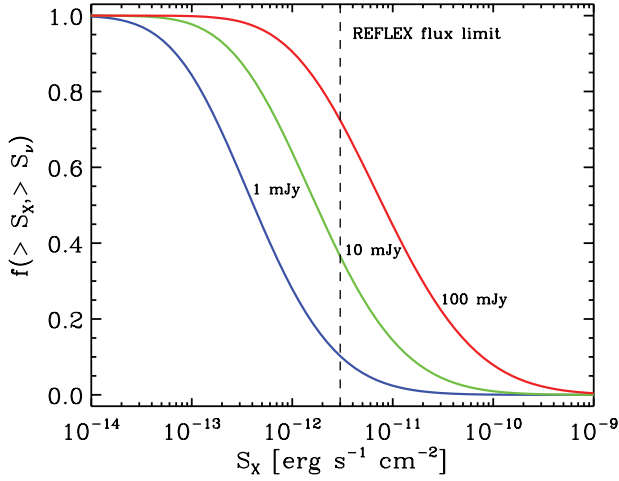
Figure 6. Cumulative fraction of clusters that host diffuse relic emission. The cumulative number is depicted as a function of X-ray flux, measured in the *ROSAT* 0.1–2.4 keV band. The curves give the cumulative number for a relic flux of 1, 10 and 100 mJy. In addition the completeness limit of the REFLEX cluster sample is given.

and X-ray catalogues, the NORAS and REFLEX cluster catalogues are well suited to identifying luminous relics. In contrast, for faint relics of about 10 mJy only ~40 per cent of the hosting clusters are expected to have fluxes above the REFLEX X-ray flux limit. This means that if upcoming surveys allow the detection of diffuse radio structures with fluxes of about 1 mJy then significantly deeper X-ray cluster catalogues will be needed to identify the majority of radio relics.

In a similar way we can determine the cumulative fraction of clusters that host diffuse relic emission as a function of radio flux. To this end, we introduce the fraction of galaxy clusters with detectable relics at a given mass and redshift:

$$f_\phi(M, z) = \int_{-\infty}^{\infty} p(P_\nu, M, z)\, \phi(S_\nu)\, \mathrm{d}\log P_\nu, \qquad (16)$$

where ϕ is the discovery probability introduced earlier. Note that for $w \to 0$ we can mimic a Heaviside function, i.e. only relics above S_ν^{eff} are detected. We can now determine the cumulative fraction of clusters hosting radio relics per X-ray luminosity bin, $\Delta \log L_X$, as follows:

$$F_\nu(> S_\nu^{\mathrm{eff}}, L_X) = \frac{1}{N_\nu(L_X)} \int_0^\infty n_{M,f} \frac{\mathrm{d}\log M}{\mathrm{d}\log L_X} \frac{\mathrm{d}V_c}{\mathrm{d}z}\, \mathrm{d}z, \qquad (17)$$

where $n_{M,f} := n_M f_\phi(M, z)$ and the normalization factor $N_\nu(L_X)$ is given by the condition $F_\nu(>0, L_X) = 1$. Fig. 7 shows the cumulative fraction for different cluster X-ray luminosities. As expected, only a small fraction of clusters show radio relics for the current detection limits of about 10 mJy. The fraction decreases strongly with the cluster X-ray luminosity. For instance, ~20 per cent of clusters with an X-ray luminosity of about 3×10^{45} erg s^{-1} are expected to host a relic with a flux of 10 mJy or brighter, while only ~0.3 per cent of clusters with 3×10^{44} erg s^{-1} are expected to do so. Note that in equation (17) we have assumed that *all* clusters with a given X-ray luminosity can be detected. To compare the result with X-ray-selected cluster samples, we need to introduce an X-ray flux limit. As a result, a large number of faint relics residing in distant clusters fall below the flux limit.

In a recent work van Weeren et al. (2011c) selected 544 clusters from the NORAS (Böhringer et al. 2000) and REFLEX (Böhringer et al. 2004) cluster samples with an X-ray flux above
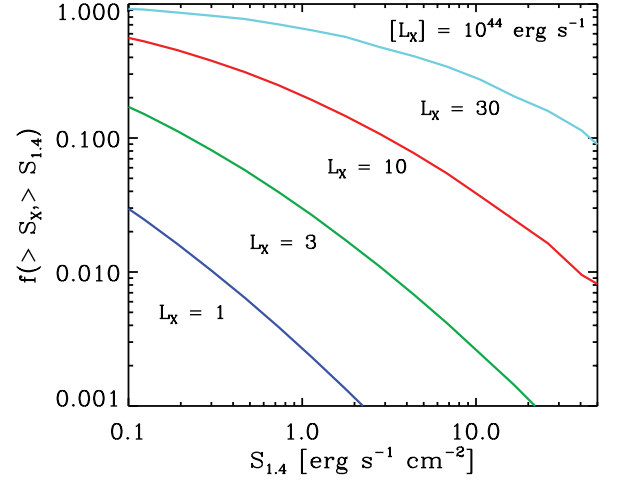

Figure 7. Cumulative fraction of clusters with relics as a function of radio flux. The cumulative number is depicted for four different X-ray luminosities.

3×10^{-12} erg s^{-1} cm^{-2} and located outside the Galactic plane. Up to this flux the REFLEX sample is virtually complete. On the other hand, the NORAS sample is almost 50 per cent complete. Interestingly, these authors show that 16 out of the 544 clusters of the combined list contain at least one radio relic and found evidence for an increase in the fraction of clusters that host relics with cluster X-ray luminosity and redshift.

Equation (17) allows us to determine the fraction of clusters with relics. The X-ray flux limit imposes an upper limit on the redshift integral, i.e. allowed redshifts must fulfil the condition $z < z(S_X^{\mathrm{th}}, L_X)$. First we wish to reproduce the $\mathrm{d}N_{\mathrm{cl}}/\mathrm{d}L_X$ and $\mathrm{d}N_{\mathrm{cl}}/\mathrm{d}z$ distributions of the cluster sample selected in van Weeren et al. (2011c). To this end we rewrite equation (17) as follows:

$$\frac{\mathrm{d}N_{\mathrm{cl}}}{\mathrm{d}L_X} = f_s \int_0^{z_{\mathrm{th}}} n_M \frac{\mathrm{d}\log M}{\mathrm{d}L_X} \frac{\mathrm{d}V_c}{\mathrm{d}z}\, \mathrm{d}z \qquad (18)$$

and

$$\frac{\mathrm{d}N_{\mathrm{cl}}}{\mathrm{d}z} = f_s \int_{L_X^{\mathrm{th}}}^\infty n_M \frac{\mathrm{d}\log M}{\mathrm{d}L_X} \frac{\mathrm{d}V_c}{\mathrm{d}z}\, \mathrm{d}L_x, \qquad (19)$$

where N_{cl} is the number of clusters and f_s indicates the sky fraction covered by the selected cluster sample, which we estimate to be 35 per cent.[1] The integration boundaries, $z_{\mathrm{th}}(S_X^{\mathrm{th}}, L_X)$ and $L_X^{\mathrm{th}}(S_X^{\mathrm{th}}, z)$ are obtained from the flux limit in the survey (see equation 1). To perform the integration we need to relate cluster mass and X-ray luminosity. We assess the cluster luminosity and redshift distributions by choosing an appropriate $L_X(M)$ relation. Recently, Pratt et al. (2009) investigated cluster scaling relations in detail. They provide best-fitting parameters for $L_{X,500}$–M_{500}, where both quantities are measured within R_{500}. However, our sample differs in several respects from theirs: (i) the halo mass function, n_M, is given for M_{200}, (ii) we do not extrapolate the luminosities to R_{500}, (iii) our sample extends up to $z \sim 0.5$ while Pratt et al. (2009) use only

---

[1] The sky fraction is estimated by $f_{\mathrm{sky}} \times f_{\mathrm{int}} \times (1 - f_{\mathrm{gal}})$, where f_{sky} is the sky fraction covered by the survey that overlaps NVSS, f_{int} is the completeness of the survey and f_{gal} is the fraction of clusters located at a galactic latitude lower than 20°. For NORAS and REFLEX we assume 50 per cent, 50 per cent and 33 per cent and 34 per cent, 90 per cent and 33 per cent for these quantities respectively. The sum of the two contributions leads to the estimated value.
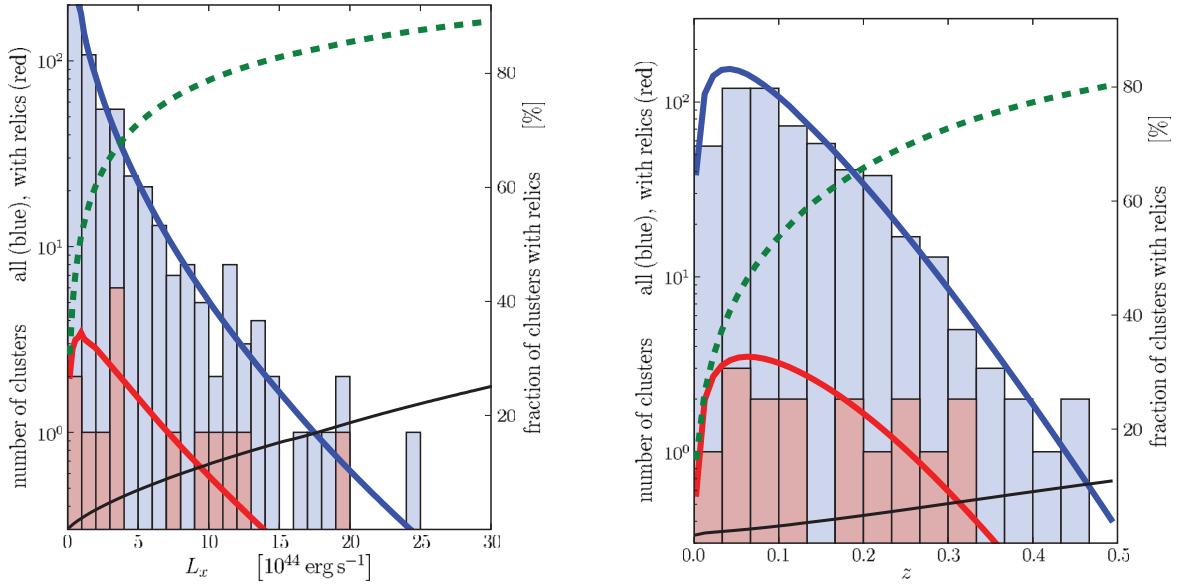
Figure 8. Luminosity (left panel) and redshift (right panel) distributions of X-ray clusters in the NORAS+REFLEX sample with and without radio relics (in the online article, red and blue histograms respectively). Solid lines (blue and red in the online article) show the distributions expected in our model, while the black solid line shows the fraction of clusters with relics (ratio between the red and blue solid lines in the online article). The dashed lines (green in the online article) show the expected fraction of clusters with relics for the NORAS sample in the upcoming LOFAR–Tier 1–120 MHz survey (see Section 4.5).

clusters with $z < 0.2$ and (iv) we use a slightly different value for Ω_M. Adopting the scaling relation

$$\frac{L_X}{5 \times 10^{43}\,\text{erg s}^{-1}} = E(z)^{7/3} \left(\frac{M_{200}}{3.4 \times 10^{14}\,h^{-1}\,M_\odot}\right)^{1.55}, \qquad (20)$$

with $E(z) = \sqrt{\Omega_M(1+z)^3 + \Omega_\Lambda}$ we are able to reproduce the observed distributions reasonably well (see Fig. 8).

To compute the abundance of clusters that actually host a detectable relic we have to use $n_{M,f} = n_M f(M, z)$ instead of n_M in equations (18) and (19). Fig. 8 (solid lines, red in the online article) shows the resulting X-ray luminosity and redshift distributions. Note that here we use a lower effective sensitivity and smaller width in $\phi(S_\nu)$ because the clusters are *known*. As discussed above, we may miss the discovery of a bright relic because the cluster has not yet been identified. For instance, the double relic in PLCK G287.0 was discovered only after the detection of the hosting cluster with the *Planck* satellite, even if the diffuse emission is clearly visible in NVSS. Since we consider here the relics in the NORAS+REFLEX sample, all clusters are known by construction. We model the discovery probability in the following way: (i) we argue that the width is smaller than for the overall sample, so we take $w = 0.2$, (ii) we adjust $S_{1.4}^{\text{eff}}$ to reproduce the fraction of clusters with relics found in the sample; using $S_{1.4}^{\text{eff}} = 27$ mJy we obtain a fraction of 3 per cent. Hence, the effective sensitivity adopted corresponds to 60 times the root-mean-square (r.m.s.) noise level in the NVSS survey. In this way we find that the fraction of relics in an X-ray flux-limited cluster sample should indeed increase with X-ray luminosity and redshift, as shown in Fig. 8. The redshift distribution is a crucial test for the mean radio-power scaling parameter C_z.

4.5 Predictions for upcoming surveys

In Table 3 we have summarized specifications for planned surveys with LOFAR and the WSRT. We would like to give some plausible estimates for the expected number of relics to be discovered by upcoming radio surveys. However, we have to remember that there

may be several uncertainties difficult to quantify. As we already mentioned, the determination of $p(P_\nu, M, z)$ is affected by the limitations of our simulation and by the adopted physical model used to relate the Mach number to the relic radio power. However, since we are able to reproduce the trends found for the NORAS+REFLEX sample, we conclude that our approach has resulted in a reasonable set of parameters. In the present paper we use the radio-relic probability density estimated from the MareNostrum simulation and leave more extensive modelling of the radio-power emission for future work.

To compute number counts for future surveys, we also need to assess the discovery probability for each survey. Since it is beyond the scope of this work to model this in detail, we simply adopt a conservative approach: we assume that the NVSS detection parameters hold similarly for the upcoming surveys, i.e. we take $w = 0.8$ (detection/non-detection transition of the instrument) and $b := S_\nu^{\text{eff}}/\sigma_\nu \sim 200$ (ratio of the effective sensitivity of the overall relic sample to the survey noise) as our fiducial parameters. The last condition means that for half of the clusters which host diffuse radio emission with a flux above 200 times the noise level of the survey, a radio relic will be detected. At this point, an important remark needs to be made in relation to the sensitivity per beam achieved by a given radio telescope. The next generation of radio surveys will presumably increase their beam resolution at least by a factor of a few. In principle, for some of the relics this could imply the requirement of higher b values than assumed here, which may lead to an overestimation of the predicted number counts. For instance, in its final configuration the LOFAR telescope is expected to reach an angular resolution of ∼5 arcsec. However, since this instrument has many short baselines it is always possible to smooth images down to typical NVSS resolution values (i.e. ∼45 arcsec) without increasing the resulting r.m.s. sensitivity too much. Nevertheless, we have to keep in mind that the final predicted number counts will depend on the adopted radio-power scalings and detection parameters. For instance, in the case of the LOFAR–Tier 1–120 MHz survey, if we let the effective detection threshold vary in the

Table 3. Properties of various present and upcoming radio surveys. For LOFAR and WODAN, different configurations are also shown. The columns correspond to name of the radio survey, observing frequency, survey noise level, observed sky area (or declination limit), corresponding sky fraction and approximate number of expected relics using our set of fiducial parameters as a function of redshift for magnetic models 'a' and 'b' (in brackets). It is worth noting that these are only plausible estimates for upcoming radio surveys but are not meant to be definitive values (see Section 4.5).

Survey	ν_{obs} [MHz]	σ_ν [mJy]	Area [deg^2]	f_s	Number of relics $(0 < z < 0.3)$	Number of relics $(0.3 < z < 0.5)$	Number of relics $(0.5 < z < 1)$	Number of relics $(z > 1)$
NVSS	1400	0.45	$\delta > -40°$	0.82	23 (26)	7 (6)	5 (3)	0 (0)
WENSS	325	3.6	$\delta > 28.5°$	0.34	8 (9)	2 (2)	1 (1)	0 (0)
LOFAR–Tier 1	60	1.0	20626	0.5	260 (365)	155 (170)	160 (140)	35 (23)
	120	0.1	20626	0.5	850 (1310)	640 (800)	810 (840)	240 (190)
	210	0.065	783	0.019	27 (41)	19 (24)	24 (24)	7 (5)
LOFAR–Tier 2	60	0.25	1184	0.029	46 (70)	34 (42)	43 (44)	12 (10)
	120	0.025	239	0.006	27 (45)	24 (34)	37 (44)	14 (13)
	210	0.016	78	0.0019	7 (12)	6 (9)	10 (11)	3 (3)
LOFAR–Tier 3	150	0.0062	30	0.0007	7 (13)	7 (11)	12 (17)	6 (6)
WODAN	1400	0.01	$\delta > 30°$	0.33	340 (510)	230 (275)	270 (265)	70 (50)
		0.005	1000	0.024	42 (66)	32 (41)	41 (43)	12 (10)

range $b = 150$–300, keeping the remaining parameters fixed, our predictions will increase (decrease) by a factor of two (a half) with respect to the prediction corresponding to $b \sim 200$. Similarly, one could assess the impact of varying some of the radio-power scaling parameters while keeping the rest unchanged. In particular, if we let the slope of the scaling with cluster mass vary in the range $C_M = 1.5$–3.5, we get brighter (fainter) relics located in clusters with masses below (above) $10^{14.5} h^{-1} M_\odot$. The predictions in this case will also increase (decrease) by a similar amount to before.

For calculation purposes here we use the radio-power scalings derived from the simulation assuming the fiducial detection parameters presented above. Table 3 gives the total number of expected relics up to $z = 0.3$, as well as relics with $0.3 < z < 0.5, 0.5 < z < 1$ and $z > 1$ for magnetic models 'a' and 'b' (in brackets). For $z > 1$, models with higher magnetic fields would generally produce fewer radio relics as a consequence of the resulting redshift evolution. Under these assumptions we expect that the LOFAR–Tier 1–120 MHz survey and WODAN large sky coverage survey should reveal several thousand radio relics, due to the huge improvement in sensitivity that will presumably be achieved by these surveys. However, a given survey may provide candidates for radio relics by cross-correlation with positions of known galaxy clusters. This means that deep follow-up observations may be needed to confirm radio relics in the clusters. Interestingly, within the context of our simple scaling for the magnetic field, we also expect a significant number of relics with $z > 0.5$ and $z > 1$ to be detected. The actual number of relics at high redshift will in particular serve to constrain the redshift evolution of magnetic fields in clusters, allowing us to refine our model prescriptions further.

As noted above, the number of relics detected in upcoming surveys will crucially depend on the cluster data base used to correlate candidates displaying diffuse radio emission with known cluster positions. As a consequence, the final number of unambiguously identified relics could be below our model expectations. To quantify this, we estimate how many relics LOFAR should find in the Tier 1–120 MHz configuration for the NORAS cluster sample introduced before. Note that the LOFAR survey and the NORAS sample both cover the north sky. Based on the effective sensitivity found in the previous section for relics in this galaxy cluster sample we adopt here a flux threshold 60 times that of the r.m.s. noise level of the LOFAR–Tier 1–120 MHz survey ($S_{1.4}^{eff}/\sigma_{Tier 1}$), which results in an effective sensitivity of 6 mJy (see dashed lines in Fig. 8). We
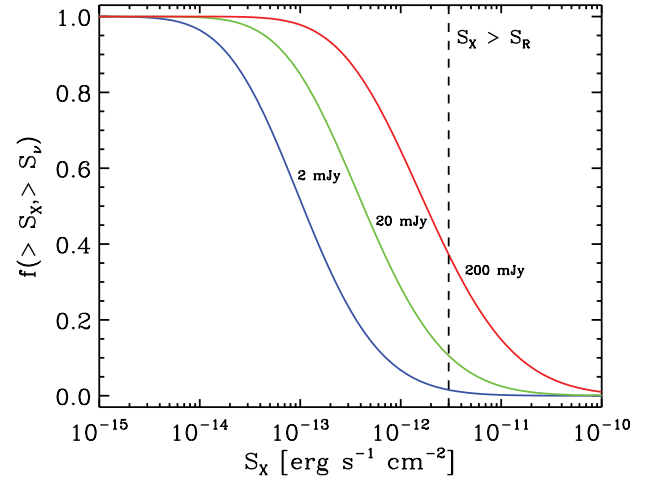

Figure 9. Same as Fig. 6 but with specifications for the LOFAR–Tier 1–120 MHz survey: $\nu_{obs} = 120$ MHz and an effective sensitivity $S_{1.4}^{eff} = 20$ mJy. The curves give the cumulative number for a relic flux of 2, 20 and 200 mJy. The X-ray completeness limit of the REFLEX cluster sample, $S_R = 3 \times 10^{-12}$ erg s^{-1} cm^{-2}, is also shown as a vertical dashed line.

find that LOFAR should discover relics in more than 50 per cent of the clusters. In the case of luminous clusters, the fraction can be as high as 90 per cent.

Using equation (15), we can also estimate the required sensitivity in X-ray surveys to find at least a fraction of the relics that can potentially be discovered in a radio survey. Fig. 9 indicates that for relics with 20 MJy in the LOFAR–Tier 1–120 MHz survey, about 50 per cent of the relics might be identified by cross-correlation if the X-ray surveys are complete up to at least 4×10^{-13} erg s^{-1} cm^{-2} (in doing this calculation we have used magnetic model 'a', as in the previous section). Hence, an all-sky X-ray catalogue with an X-ray flux limit one order of magnitude below that of the REFLEX sample is necessary to identify a considerable fraction of the relics.

5 SUMMARY

Radio relics are believed to trace merger shock fronts in galaxy clusters. The radio luminosity of shock fronts depends strongly on the Mach number of the shock, but also on the size of the front and

on the magnetic field present in the downstream region. Even if in every cluster there are shock fronts related to past merger events, the actual radio luminosity caused by the shocks may vary strongly, from no detectable radio emission at all to the presence of luminous radio relics. To describe the large spread of radio luminosities more formally, we have introduced the *radio-power probability distribution*, $p(P_\nu, M, z)$, aimed at assessing the likelihood of relics in galaxy clusters with a given mass and redshift at a given frequency. We use the MareNostrum Universe simulation to estimate the probability distribution. To this aim, we selected the 500 most massive clusters at five different redshifts up to $z = 1$ to detect shock fronts in assembling galaxy clusters. Then, we apply the scheme developed by Hoeft et al. (2008) for estimating their radio-relic luminosity. Based on the distribution of radio-relic luminosities of the simulated clusters, we conclude that the radio-power probability is well approximated by a log-normal distribution. Moreover, using our galaxy cluster samples we are able to estimate how the radio-relic distributions scale with cluster mass, redshift and observing frequency.

Using the radio-power probability distribution, we wish to determine the relic number counts, $N(>S_\nu)$. Basically this is given by a convolution of the probability distribution and the dark matter halo mass function. However, radio relics are not straightforwardly identified in radio observations and therefore even luminous relics are possibly present in radio catalogues, but not yet identified as relics. For instance, the relics in 1RXS 06+42 and in CIZA 2242 are bright and are present in the WENSS catalogue but have only recently been reported as relics. We therefore introduce the discovery probability as a function of radio flux, $\phi(S_\nu)$. The number counts are obtained by a convolution of all three: the halo mass function, the radio-power probability distribution and the discovery probability.

It is important to remark that it is not possible to *predict* radio-flux number counts of relics purely from cosmological simulations. In this regard, a major source of uncertainty is the efficiency of electron acceleration at the shock front. We therefore use the observed relic number counts to determine the reference normalization for the radio-power probability distribution.

The resulting framework allows us to estimate the number of detectable relics in upcoming radio surveys. In the following we summarize our main conclusions.

(i) To evaluate the MareNostrum Universe simulation, we *assumed* an electron acceleration efficiency $\xi_e = 0.005$ and two different magnetic field scalings with local electron density in the simulation. Normalizing the radio-power probability distribution by the list of known NVSS relics resulted in lower values for the reference radio power, which can be interpreted as evidence for a low electron acceleration efficiency. In particular, we find that $\xi_e \lesssim 0.001$. According to the magnetic scaling proposed by Bonafede et al. (2010) in the case of the Coma cluster (model 'b'), the acceleration efficiency could easily reach values of $\xi_e \sim 10^{-5}$. However, there are many uncertainties that may affect the P_0 value, e.g. the actual discovery probability.

(ii) After normalizing the radio-relic number counts, $N(>S_\nu)$, we split the obtained number counts into redshift bins. As a result we expect more relics for $z > 0.3$ than are observed. This might indicate that the $B(n_e)$ relations assumed in the simulation show an additional dependence on redshift. However, magnetic model 'b' seems to agree better with observational results, which would point toward $\gtrsim \mu G$ magnetic fields in the location of radio relics. We consider this approach as a very promising diagnostic of the evolution of magnetic

fields in galaxy clusters, but larger relic samples are needed to draw any robust conclusion.

(iii) The observed relic number counts are reasonably reproduced assuming an effective sensitivity of 100 mJy. Candidates for many relics may have been first identified in the NVSS survey, which has an r.m.s. noise level of 0.45 mJy. We therefore adopt the suggestion that the effective sensitivity for finding relics is generally about 200 times the r.m.s. noise of a survey. We apply this to the specifications of the proposed LOFAR and APERTIF surveys. Under these assumptions we find that the LOFAR–Tier 1–120 MHz survey has the potential to find more than a thousand radio relics.

(iv) More than 50 per cent of the relics expected to be found with the LOFAR–Tier 1–120 MHz survey should reside in clusters with $z > 0.3$ and there should be even more than 100 relics in clusters with $z > 1$. Hence, in principle this survey will allow us to discover sufficient relics to analyse the evolution of magnetic fields in clusters in a statistical way.

(v) To discover a relic confidently, the clusters that host the diffuse radio emission need to be identified. Many of the relics that are detectable by the LOFAR–Tier 1–120 MHz survey may reside in faint clusters. More precisely, we predict that about 50 per cent of the relics with 20 mJy will reside in clusters with an X-ray flux below 4×10^{-13} erg s^{-1} cm^{-2}.

(vi) Following van Weeren et al. (2011c), we study an X-ray flux galaxy cluster sample based on the NORAS+REFLEX catalogues. About 4 per cent of the galaxy clusters in the sample host radio relics. This value is significantly lower than the one obtained for the overall sample, since we consider only known clusters here. We found that we can reproduce the relic fraction assuming an effective sensitivity of 27 mJy at 1.4 GHz. As discussed in van Weeren et al. (2011c), we also find that the fraction of clusters hosting a relic increases with cluster X-ray luminosity and redshift.

(vii) We expect that the LOFAR–Tier 1–120 MHz survey will find radio relics in around 50 per cent of the NORAS+REFLEX clusters. Furthermore, for the most massive clusters this fraction can be as high as 90 per cent.

REFERENCES

Araya-Melo P. A., Aragón-Calvo M. A., Brüggen M., Hoeft M., 2011, MNRAS, submitted
Bagchi J., Enßlin T. A., Miniati F., Stalin C. S., Singh M., Raychaudhury S., Humeshkar N. B., 2002, New Astron., 7, 249

Bagchi J., Durret F., Neto G. B. L., Paul S., 2006, Sci, 314, 791
Bagchi J. et al., 2011, ApJ, 736, 8
Battaglia N., Pfrommer C., Sievers J. L., Bond J. R., Enßlin T. A., 2009, MNRAS, 393, 1073
Blandford R., Eichler D., 1987, Phys. Rep., 154, 1
Böhringer H. et al., 2000, ApJS, 129, 435
Böhringer H. et al., 2004, A&A, 425, 367
Bonafede A., Giovannini G., Feretti L., Govoni F., Murgia M., 2009, A&A, 494, 429
Bonafede A., Feretti L., Murgia M., Govoni F., Giovannini G., Dallacasa D., Dolag K., Taylor G. B., 2010, A&A, 513, 30
Brown S., Rudnick L., 2009, AJ, 137, 3158
Brown S., Duesterhoeft J., Rudnick L., 2011, ApJ, 727, L25
Cassano R., Brunetti G., Röttgering H. J. A., Brüggen M., 2010, A&A, 509, A68
Clarke T. E., Ensslin T. A., 2006, AJ, 131, 2900
Cohen A. S., Lane W. M., Cotton W. D., Kassim N. E., Lazio T. J. W., Perley R. A., Condon J. J., Erickson W. C., 2007, AJ, 134, 1245
Condon J. J., Cotton W. D., Greisen E. W., Yin Q. F., Perley R. A., Taylor G. B., Broderick J. J., 1998, AJ, 115, 1693
David L. P., Forman W., Jones C., 1999, ApJ, 519, 533
Dolag K., Grasso D., Springel V., Trachev I., 2005, in Sjouwerman L. O., Dyer K. K., eds, X-Ray and Radio Connections. http://www.aoc.nrao.edu/events/xraydio/index.shtml
Dolag K., Bykov A. M., Diaferio A., 2008, Space Sci. Rev., 134, 311
Drury L. O., 1983, Rep. Progr. Phys., 46, 973
Ebeling H., Mullis C. R., Tully R. B., 2002, ApJ, 580, 774
Edge A. C., Ebeling H., Bremer M., Röttgering H., van Haarlem M. P., Rengelink R., Courtney N. J. D., 2003, MNRAS, 339, 913
Edmon P. P., Kang H., Jones T. W., Ma R., 2011, MNRAS, 414, 3521
Enßlin T. A., Brüggen M., 2002, MNRAS, 331, 1011
Enßlin T. A., Gopal-Krishna, 2001, A&A, 366, 26
Enßlin T. A., Röttgering H., 2002, A&A, 396, 83
Enßlin T. A., Biermann P. L., Klein U., Kohle S., 1998, A&A, 332, 395
Feretti L., Fusco-Femiano R., Giovannini G., Govoni F., 2001, A&A, 373, 106
Feretti L., Bacchi M., Slee O. B., Giovannini G., Govoni F., Andernach H., Tsarevsky G., 2006, MNRAS, 368, 544
Giacintucci S. et al., 2008, A&A, 486, 347
Giovannini G., Feretti L., 2000, New Astron., 5, 335
Giovannini G., Feretti L., Stanghellini C., 1991, A&A, 252, 528
Giovannini G., Tordi M., Feretti L., 1999, New Astron., 4, 141
Giovannini G., Bonafede A., Feretti L., Govoni F., Murgia M., Ferrari F., Monti G., 2009, A&A, 507, 1257
Giovannini G., Bonafede A., Feretti L., Govoni F., Murgia M., 2010, A&A, 511, L5
Giovannini G., Feretti L., Girardi M., Govoni F., Murgia M., Vacca V., Bagchi J., 2011, A&A, 530, L5
Gottlöber S., Yepes G., 2007, ApJ, 664, 117
Govoni F., Feretti L., 2004, Int. J. Modern Phys. D, 13, 1549
Govoni F., Feretti L., Giovannini G., Böhringer H., Reiprich T. H., Murgia M., 2001, A&A, 376, 803
Govoni F., Murgia M., Giovannini G., Vacca V., Bonafede A., 2011, A&A, 529, A69
Grasso D., Rubinstein H. R., 2001, Phys. Rep., 348, 163
Hoeft M., Brüggen M., 2007, MNRAS, 375, 77
Hoeft M., Brüggen M., Yepes G., Gottlöber S., Schwope A., 2008, MNRAS, 391, 1511
Jones F. C., Ellison D. C., 1991, Space Sci. Rev., 58, 259
Kempner J. C., Sarazin C. L., 2001, ApJ, 548, 639
Kempner J. C., Blanton E. L., Clarke T. E., Enßlin T. A., Johnston-Hollitt M., Rudnick L., 2004, in Reiprich T., Kempner J., Soker N., eds, The Riddle of Cooling Flows in Galaxies and Clusters of Galaxies, p. 335. http://www.astro.virginia.edu/coolflow/
Keshet U., 2010, ArXiv e-print
Klypin A., Gottlöber S., Kravtsov A. V., Khokhlov A. M., 1999, ApJ, 516, 530

Kocevski D. D., Ebeling H., Mullis C. R., Tully R. B., 2007, ApJ, 662, 224
Komatsu E. et al., 2011, ApJS, 192, 18
Kuchar P., Enßlin T. A., 2011, A&A, 529, 13
Landau L. D., Lifshitz E. M., 1959, in Landau L. D., Lifshitz E. M., eds, Fluid Mechanics. Pergamon Press, Oxford
Macario G., Markevitch M., Giacintucci S., Brunetti G., Venturi T., Murray S. S., 2011, ApJ, 728, 82
Malkov M. A., O'C Drury L., 2001, Rep. Progr. Phys., 64, 429
Markevitch M., 2010, ArXiv e-print
Markevitch M., Forman W. R., Sarazin C. L., Vikhlinin A., 1998, ApJ, 503, 77
Markevitch M. et al., 2003, ApJ, 586, L19
Monaghan J. J., 1992, ARA&A, 30, 543
Nakazawa K. et al., 2009, PASJ, 61, 339
Ogrean G. A., Brüggen M., van Weeren R., Simionescu A., Röttgering H., Croston J. H., 2011, MNRAS, 414, 1175
Pfrommer C., Springel V., Enßlin T. A., Jubelgas M., 2006, MNRAS, 367, 113
Pizzo R. F., de Bruyn A. G., 2009, A&A, 507, 639
Pizzo R. F., de Bruyn A. G., Feretti L., Govoni F., 2008, A&A, 481, L91
Popesso P., Böhringer H., Brinkmann J., Voges W., York D. G., 2004, A&A, 423, 449
Pratt G. W., Croston J. H., Arnaud M., Böhringer H., 2009, A&A, 498, 361
Reid A. D., Hunstead R. W., Lemonon L., Pierre M. M., 1999, MNRAS, 302, 571
Reiprich T. H., Böhringer H., 2002, ApJ, 567, 716
Rengelink R. B., Tang Y., de Bruyn A. G., Miley G. K., Bremer M. N., Roettgering H. J. A., Bremer M. A. R., 1997, A&AS, 124, 259
Röttgering H. J. A., Wieringa M. H., Hunstead R. W., Ekers R. D., 1997, MNRAS, 290, 577
Shen S., Kauffmann G., von der Linden A., White S. D. M., Best P. N., 2008, MNRAS, 389, 1074
Skillman S. W., Hallman E. J., O'Shea B. W., Burns J. O., Smith B. D., Turk M. J., 2011, ApJ, 735, 96
Slee O. B., Roy A. L., Murgia M., Andernach H., Ehle M., 2001, AJ, 122, 1172
Springel V., 2005, MNRAS, 364, 1105
Springel V., Yoshida N., White S. D. M., 2001, New Astron., 6, 79
Subrahmanyan R., Beasley A. J., Goss W. M., Golap K., Hunstead R. W., 2003, AJ, 125, 1095
Tinker J., Kravtsov A. V., Klypin A., Abazajian K., Warren M., Yepes G., Gottlöber S., Holz D. E., 2008, ApJ, 688, 709
van Weeren R. J., Röttgering H. J. A., Brüggen M., Cohen A., 2009a, A&A, 505, 991
van Weeren R. J. et al., 2009b, A&A, 506, 1083
van Weeren R. J., Röttgering H. J. A., Brüggen M., Cohen A., 2009c, A&A, 508, 75
van Weeren R. J., Röttgering H. J. A., Brüggen M., Hoeft M., 2010, Sci, 330, 347
van Weeren R. J., Röttgering H. J. A., Brüggen M., 2011a, A&A, 527, A114
van Weeren R. J., Hoeft M., Röttgering H. J. A., Brüggen M., Intema H. T., van Velzen S., 2011b, A&A, 528, A38
van Weeren R. J., Brüggen M., Röttgering H. J. A., Hoeft M., Nuza S. E., Intema H. T., 2011c, A&A, 533, A35
Venturi T., Giacintucci S., Brunetti G., Cassano R., Bardelli S., Dallacasa D., Setti G., 2007, A&A, 463, 937
Venturi T., Giacintucci S., Dallacasa D., Cassano R., Brunetti G., Bardelli S., Setti G., 2008, A&A, 484, 327
Venturi T., Giacintucci G., Dallacasa D., Brunetti G., Cassano R., Macario G., Athreya R., 2011, MNRAS, 414, L65
Vikhlinin A., Markevitch M., Murray S. S., 2001, ApJ, 551, 160
Vogt C., Enßlin T. A., 2003, A&A, 412, 373
Völk H. J., Atoyan A. M., 2000, ApJ, 541, 88

This paper has been typeset from a TEX/LATEX file prepared by the author.